Poly(ADP-ribose) Polymerase-1 Dimerizes at a 5′ Recessed DNA End *in Vitro*: A Fluorescence Study[†]

Emmanuelle Pion,[‡] Elisa Bombarda,*,[‡] Patrick Stiegler,[§] G. Matthias Ullmann,[∥] Yves Mély,[‡] Gilbert de Murcia,[§] and Dominique Gérard[‡]

UMR 7034 du CNRS, Laboratoire de Pharmacologie et Physico-Chimie des Interactions Cellulaires et Moléculaires, Faculté de Pharmacie, Université Louis Pasteur, 74, Route du Rhin, F-67401 Illkirch Cedex, France, UPR 9003 du CNRS, Ecole Supérieure de Biotechnologie de Strasbourg, Boulevard Sébastien Brant, F-67400 Illkirch, France, and IWR-Biocomputing, University of Heidelberg, Im Neuenheimer Feld, 368 69120 Heidelberg, Germany

ABSTRACT: Activation of poly(ADP-ribose) polymerase-1 (PARP-1) is an immediate cellular reaction to DNA strand breakage as induced by alkylating agents, ionizing radiation, or oxidants. The resulting formation of protein-bound poly(ADP-ribose) facilitates survival of proliferating cells under conditions of DNA damage probably via its contribution to DNA base excision repair. In this study, we investigated the association of the amino-terminal DNA binding domain of human PARP-1 (hPARP-1 DBD) with a 5′ recessed oligonucleotide mimicking a telomeric DNA end. We used the fluorescence of the Trp residues naturally occurring in the zinc finger domain of hPARP-1 DBD. Fluorescence intensity and fluorescence anisotropy measurements consistently show that the binding stoichiometry is two proteins per DNA molecule. hPARP-1 was found to bind the 5′ recessed DNA end with a binding constant of $\sim10^{14}$ M^{-2} if a cooperative binding model is assumed. These results indicate that hPARP-1 DBD dimerizes during binding to the DNA target site. A footprint experiment shows that hPARP-1 DBD is asymmetrically positioned at the junction between the double-stranded and the single-stranded telomeric repeat. The largest contribution to the stability of the complex is given by nonionic interactions. Moreover, time-resolved fluorescence measurements are in line with the involvement of one Trp residue in the stacking interaction with DNA bases. Taken together, our data open new perspectives for interpretation of the selective binding of hPARP-1 to the junction between double- and single-stranded DNA.

The presence of damaged DNA in the cell activates signal transduction pathways that trigger cell cycle arrest and repair mechanisms, which ultimately lead to cell survival or programmed cell death (*1*). Activation of poly(ADP-ribose) polymerase-1 (PARP-1, EC 2.4.2.30) is an immediate cellular response to DNA strand breakage induced by alkylating agents, ionizing radiation, or oxidants. The resulting formation of protein-bound poly(ADP-ribose) facilitates survival of proliferating cells under conditions of DNA damage because of chromatin structure opening and/or recruitment of DNA repair enzymes and factors (*2*). Evidence has emerged that this posttranslational modification is involved in the maintenance of genomic stability (*3−5*). Indeed, PARP-1 deficient mice show hypersensitivity to genotoxic stress, as well as an increased chromosomal instability following DNA damage (*6, 7*).

PARP-1 (113 kDa) is a highly conserved multifunctional enzyme whose enzymatic activity is stimulated more than 500-fold upon binding to DNA strand breaks. Its modular structure comprises three main distinct regions: the N-terminal DNA-binding domain (46 kDa) which bears two zinc fingers of the form $Cx_2Cx_{28,30}Hx_2C$ (29 kDa) acting as a molecular nick sensor (Figure 1B), the central automodification domain (22 kDa) bearing a BRCT motif and containing autopoly(ADP-ribosyl)ation sites which are implicated in the regulation of PARP−DNA interactions, and the C-terminal catalytic domain (54 kDa) which is involved in poly(ADP-ribose) synthesis upon nick binding.

Additional members of the PARP family have been identified in the past few years. In mammals, a total of 18 different cDNAs that encode new members of this emerging superfamily have now been identified in the human genome (J. C. Ame *et al.*, manuscript in preparation). They all share, to various degrees of conservation, the PARP signature, a block of 50 amino acids, generally located in their C-terminus and virtually unchanged from plants to humans, forming the catalytic site of the founding member PARP-1. Given the conservation of the C-terminal catalytic site among the whole PARP family, the elucidation of the DNA binding process of PARP-1 at the molecular level is an obligatory step not only in understanding its biological role but also in the development of activators and inhibitors raised specifically against the N-terminal nick binding function of PARP-1.

* To whom correspondence should be addressed. Telephone: +33 (0)3 90 24 42 55. Fax: +33 (0)3 90 24 43 12. E-mail: elisa@pharma.u-strasbg.fr.
[‡] Université Louis Pasteur.
[§] Ecole Supérieure de Biotechnologie de Strasbourg.
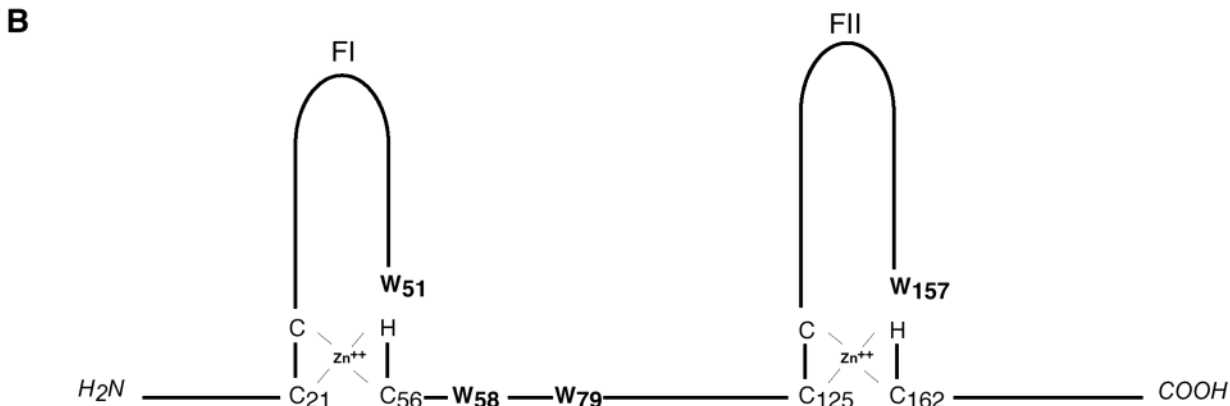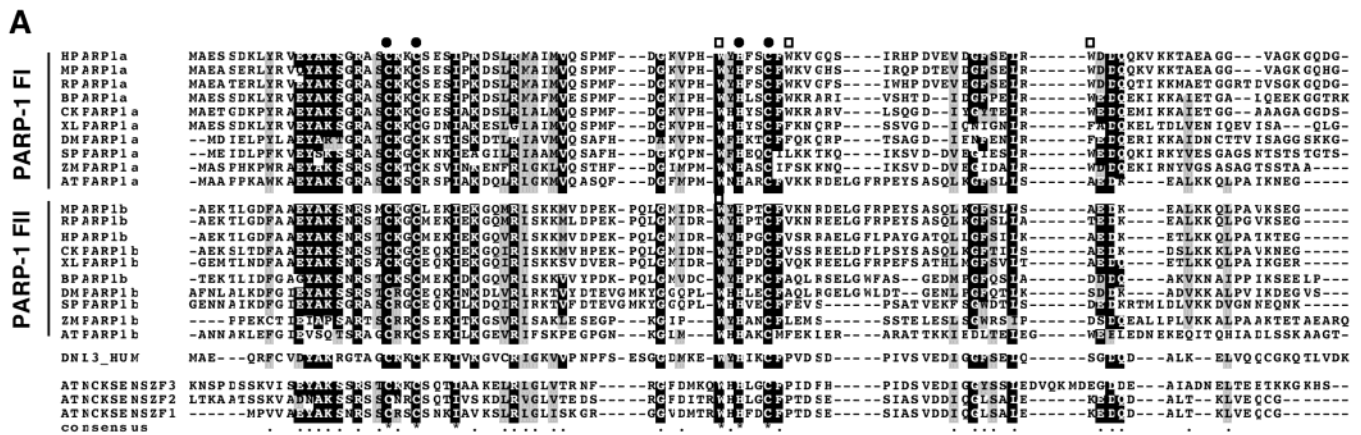[∥] University of Heidelberg.

FIGURE 1: (A) PARP-1-like zinc finger family. Comparison of the deduced amino acid sequences of the amino-terminal region of DNA ligase III (DNL3_HUM, accession number P49916) and the three zinc fingers of the nick sensing DNA 3′-phosphoesterase from *A. thaliana* (ATNCKSENZF1−3, accession number AF453835) with the N-terminal zinc finger region of PARP-1 from human (hPARP-1, accession number P09874), mouse (mPARP-1, accession number P11103), rat (rPARP-1, accession number P27008), bovine (bPARP-1, accession number P18493), chicken (ckPARP-1, accession number P26446), *Xenopus laevis* (xlPARP-1, accession number P31669), *Drosophila melanogaster* (dmPARP-1, accession number P35875), *Stichocorys peregrina* (spPARP-1, accession number D16482), *Zea mays* (zmPARP-1, accession number AF093627), and *A. thaliana* (atPARP-1, accession number AJ131705). Identical amino acid residues are boxed in black. Conserved substitutions are indicated in gray. The filled circles denote the Cys and His residues involved in the coordination of zinc, and the empty squares denote the Trp residues. (B) PARP-1 DBD structure of the N-terminal binding domain of hPARP-1 (residues 1−234). The DNA-binding domain is drawn to show two zinc-coordinated fingers (FI and FII). The four tryptophans (W51, W58, W79, and W157) are shown in bold.

The zinc finger motif of the amino terminus of the human PARP-1 DNA binding domain (hPARP-1[1] DBD) contains four Trp residues at positions 51, 58, 79, and 157. Two of them, Trp51 and Trp157, are located in the zinc fingers and are strictly conserved during evolution from *Arabidopsis thaliana* to humans (*8*) (Figure 1A). Interestingly, this zinc finger motif is also present in other base excision repair enzymes such as DNA ligase III (*9*) and the nick sensing DNA 3′-phosphoesterase from *A. thaliana* (*10*) involved in the resolution of DNA interruptions.

In the study presented here, we report the steady state and time-resolved fluorescence properties of hPARP-1 DBD by monitoring the signal of the four Trp residues present in this domain to gain information about its binding mode with a DNA target. Because of their high sensitivity to even minor changes in the physicochemical environment, Trp residues constitute suitable and powerful intrinsic fluorescence probes for investigating the interaction of proteins with various

ligands and, notably, nucleic acids (*11*). Given the recently reported connection between hPARP-1, telomerase (*12*), and some telomeric proteins (*13*), the interaction between hPARP-1 DBD and a double-stranded oligonucleotide mimicking an open telomeric DNA end was investigated with this approach.

MATERIALS AND METHODS

Materials. hPARP-1 DBD (residues 1−234) cloned in expression vector pTG161 (*14*) was overexpressed in *Escherichia coli* and affinity purified on both hydroxyapatite and DNA cellulose chromatography columns as previously described (*15*). The homogeneity of hPARP-1 DBD was ascertained by its relative molecular mass using 10% SDS−PAGE. The protein was stored at −80 °C in 20% glycerol until it was used. The hPARP-1 DBD concentration was determined on a Cary 4 spectrophotometer using an extinction coefficient of 30 620 M^{-1} cm^{-1} at 280 nm. The DNA binding buffer was made of 50 mM Tris-HCl, 100 mM NaCl, and 1 mM DTT (pH 8), if not otherwise stated. Oligonucleotides containing human telomeric repeats (TTAGGG) next to an anchor sequence bearing a *Not*I restriction site to

---

[1] Abbreviations: DTT, dithiothreitol; hPARP-1, human poly(ADP-ribose) polymerase-1; HPLC, high-performance liquid chromatography; SDS−PAGE, sodium dodecyl sulfate−polyacrylamide gel electrophoresis; BRCT, breast cancer susceptibility protein, BRCA1, C-terminus; TRF-2, TTAGGG repeat factor 2.
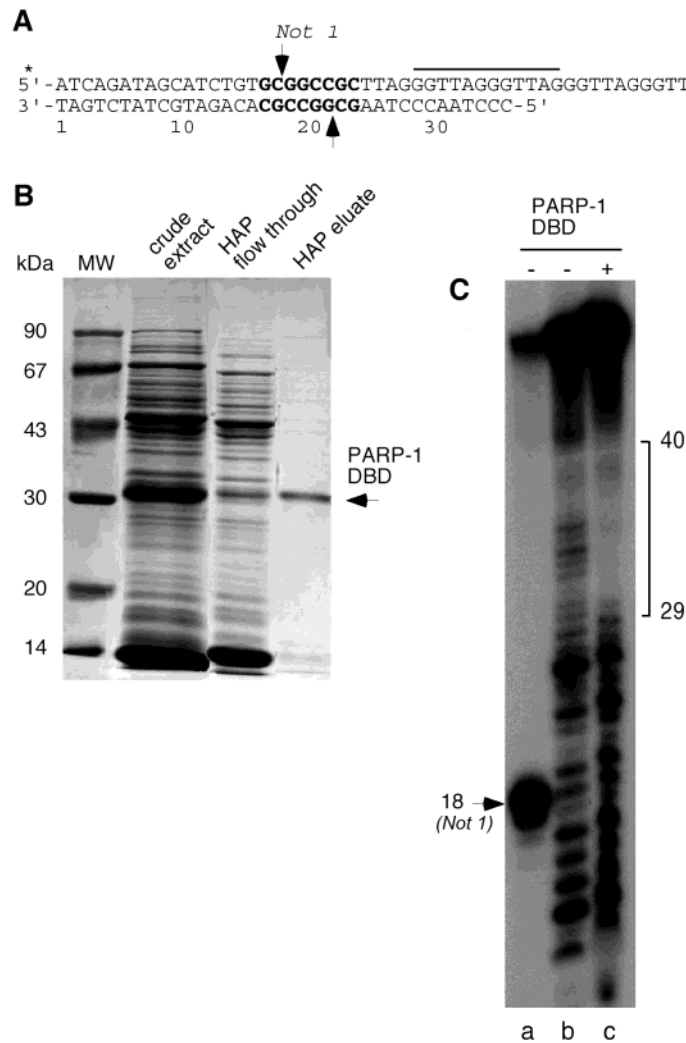
FIGURE 2: (A) Sequence of the 60 bp deoxyoligonucleotide probe containing six telomeric TTAGGG repeats and a *Not*I site for the control of annealing. The probe has a 5′ recessed telomeric end of 36 nucleotides mimicking a telomere end. The bar indicates the protected region. (B) Purification of the hPARP-1 DBD overproduced in *E. coli*. The HAP eluate lane shows the final product, after it had passed through hydroxyapatite and DNA cellulose columns, as described in Materials and Methods (*20*). (C) DNase I footprinting of hPARP-1 DBD on telomere-like structures performed according to the method of Mènissier-de Murcia et al. (*16*). The signs + and − indicate the presence and absence of hPARP-1 DBD, respectively: lane a, *Not*I restriction to confirm annealing (the arrow points to the cleaved *Not*I site); lane b, DNase I degradation products without protein; and lane c, footprint of the hPARP-1 DBD−DNA complex. The protected nucleotides are denoted with a bracket.

monitor the annealing (Figure 2A) were synthesized on a 0.2 μmol scale by IBA GmbH Nucleic Acids Product Supply (Göttingen, Germany) and purified by reverse-phase HPLC and polyacrylamide gel electrophoresis by the manufacturer. Oligonucleotide concentrations were calculated at 260 nm using extinction coefficients of 590 940 and 338 580 M^{-1} cm^{-1} for the "G" strand and the "C" strand, respectively (Figure 2A). Annealing reactions were carried out by incubating the oligonucleotides for 2.5 min at 85 °C in 50 mM Tris-HCl (pH 8.0), 300 mM NaCl, and 1 mM DTT, and then allowing them to cool slowly. The correct annealing was confirmed by the *Not*I restriction (Figure 2A).

DNase I Footprinting. Purified hPARP-1 DBD (100 ng) was immobilized onto nitrocellulose (BAS83, Schleicher & Schuel) and allowed to bind to 20 ng of 5′ ^{32}P end-labeled DNA at 0 °C in the binding buffer [50 mM Tris-HCl (pH 8.0), 150 mM NaCl, and 0.1% Nonidet P-40]. Following incubation for 1 h, the membranes were washed three times with the binding buffer at 0 °C. The membranes were then either dried and subjected to autoradiography to visualize the protein−DNA complexes or autoradiographed while wet for 1 h so that the filter-bound protein−DNA complexes could be excised and used for DNase I footprinting assays as described previously (*16*).

Steady State Fluorescence Measurements. Fluorescence emission spectra were recorded in quartz cells at 20.0 ± 0.5 °C on an SLM 48000 spectrofluorimeter. The excitation and emission bandwidths were 2 and 8 nm, respectively. The quantum yield of hPARP-1 DBD at 295 nm was determined by using L-Trp in water ($\Phi = 0.14$) as a reference (*17*). The binding of hPARP-1 DBD to DNA was monitored using the fluorescence signal of Trp residues present in the protein. Fluorescence titrations were performed by adding increasing amounts of oligonucleotide (Figure 2A) to a fixed amount of protein in 50 mM Tris-HCl (pH 8), 100 mM NaCl, and 1 mM DTT. The various molar ratios of oligonucleotide to protein were prepared as separate solutions. The excitation wavelength was set at 295 nm.

Salt-back titrations were performed by adding increasing concentrations of NaCl to the preformed complexes in separate tubes. As the plots of log K versus log[NaCl] were linear in the salt concentration range of 100−800 mM, this method allows the determination of the nonionic binding constant $K(1 M)$ and the number of ion pairs (m') between the protein and the nucleic acid in the complex, according to eq 1:

$$\log K = \log K(1 M) - \Psi_{Na^+} m' \log[NaCl] \quad (1)$$

where Ψ_{Na^+}, the fraction of Na^+ cations on average bound per phosphate group, is assumed to be 0.8, which corresponds to the average between the value of 0.71 for single-stranded DNA and the value of 0.88 for double-stranded DNA (*18*). In addition, we assumed that no anion uptake or release accompanied the binding of hPARP-1 DBD to the telomeric DNA.

Steady state anisotropy measurements were performed with a T-format SLM 8000 spectrofluorometer at 20 °C. The emitted light was monitored through 350 nm interference filters (Schott). A device built in house ensured the automatic rotation of the excitation polarizer. Increasing amounts of DNA were added to 1 μM hPARP-1 DBD under the same conditions as described above.

Time-Resolved Fluorescence Measurements. Time-resolved fluorescence measurements were performed with a time-correlated, single-photon counting technique using the stable excitation pulses provided by a pulse-picked frequency-tripled Ti−sapphire laser (Tsunami, Spectra Physics) pumped by a Millenia X laser (Spectra Physics). The temperature was maintained at 20 °C. The excitation pulses were set at 295 nm, with a repetition rate of 4 MHz. The emission was collected through a 4 nm band-pass monochromator (Jobin-Yvon H10) set at 350 nm and a polarizer set at the magic angle. The single-photon events were detected with a microchannel plate Hamamatsu R3809U photomultiplier coupled to a Philips 6954 pulse preamplifier and recorded on a multichannel analyzer (Ortec 7100) calibrated at 25.5 ps/channel. The instrumental response function was recorded with a polished aluminum reflector, and its full width at half-maximum was 40 ps. For lifetime measurements, the polarizer in the emission path was set at the magic angle (54,7°). For time-resolved anisotropy measurements, this polarizer was set in a vertical position. $I_\perp(t)$ and $I_\parallel(t)$ were recorded alternatively every 5 s, by using the vertical polarization of the excitation beam with and without the interposition of a quartz crystal rotating the beam polarization by 90°.

Time-resolved data analysis was performed using the maximum entropy method (MEM) and the Pulse5 software (*19*). For the analysis of the fluorescence decay, a distribution of 200 equally spaced lifetime values on a logarithmic scale between 0.01 and 10 ns was used. The anisotropy decay parameters were extracted from both $I_\perp(t)$ and $I_\parallel(t)$. A distribution of 200 equally spaced correlation time values on a logarithmic scale between 0.01 and 30 ns was used. In all cases, the reduced χ^2 values were close to 1.0, and the weighted residuals as well as the autocorrelation of the residuals were distributed randomly around zero, indicating an optimal fit.

In time-resolved anisotropy experiments, the rotational correlation times θ_F and θ_L associated with the local and overall motion, respectively, were deduced from two experimental times (θ_1 and θ_2) with the assumption that the local motion of Trp residues is independent of the rotational motion of the protein. Accordingly, the anisotropy at any time t is given by

$$r(t) = (r_0 - r_\infty)(\alpha e^{-t/\theta_F} + 1 - \alpha)e^{-t/\theta_L} + r_\infty \quad (2)$$

where r_0 and r_∞ are the fundamental and limiting anisotropy, respectively, and α corresponds to the fraction of depolarization to which the fast motion contributes. In our case, the anisotropy decays to zero, and thus, $r_\infty = 0$. Under these conditions, $\theta_L = \theta_2$ and $1/\theta_F = 1/\theta_1 - 1/\theta_L$. Since $\theta_1 \ll \theta_2, \theta_F \approx \theta_1$.

RESULTS

DNA Binding Properties of the hPARP-1 Zinc Finger Domain. We have previously shown that the purified human hPARP-1 DBD, overproduced in *E. coli*, is fully functional and binds specifically to a single-stranded break (*14*, *15*, *20*). The recently established link between PARP-1 and some telomeric proteins (*12*, *13*) prompted us to investigate the binding of hPARP-1 DBD to oligonucleotides bearing TTAGGG repeats forming a 5′ recessed telomeric end (Figure 2A). hPARP-1 DBD purified from *E. coli* (Figure 2B) was incubated with 5′ end-labeled telomeric probes (Figure 2A) and processed for footprinting experiments. As shown in Figure 2C, a specific binding of hPARP-1 DBD occurs at the junction between the double-stranded and single-stranded telomeric repeat. Eleven nucleotides are protected. Similar protection of the 5′ end was observed using a DNA duplex bearing a nontelomeric 5′ recessed end of 33 nucleotides, therefore confirming the affinity of hPARP-1 for 5′ ends, independent of the sequence context (data not shown).

Altogether, these results demonstrate that the open configuration of a telomeric end may constitute a specific target for hPARP-1 once the T-loop has been relaxed following DNA damage (*21*). The interaction of hPARP-1 DBD with a deoxyoligonucleotide bearing a 5′ recessed telomeric end of 36 nucleotides (Figure 2A) is further investigated by fluorescence spectroscopy.

Fluorescence Properties of hPARP-1 DBD. Preliminary experiments have shown that hPARP-1 DBD has a strong tendency to be adsorbed onto the walls of the quartz cell. This effect leads to the reduction of the concentration of fluorescent molecules in the detection volume and thus to a subsequent artifactual decrease in the magnitude of the fluorescence signal. Since either continuous stirring or mixing by cell reversal is known to favor adsorption (*22*), each solution containing the protein is prepared by gently mixing the components (a few seconds on a low-speed vortex) in separate low binding Eppendorf tubes. The protein solutions are then carefully transferred into the quartz cell using low binding tips, without further mixing. Consistent results for different protein concentrations show that protein adsorption did not significantly affect the outcome of the experiments.

hPARP-1 DBD is highly sensitive to photobleaching. Exposure to light excitation over the course of 1000 s with excitation slits of 8 nm decreased the fluorescence intensity by ~30%. To overcome this inconvenience, excitation slits of 2 nm are chosen and the excitation time is always less than 50 s.

Table 1: Fluorescence Decay Parameters and Quantum Yield of hPARP-1 DBD in the Free Form and in the Complex with the 5′ Recessed DNA End

	τ_i (ns)[a]	α_i[a]	f_i[a]	$\langle \tau \rangle$ (ns)[a]	Φ_{295}[b]
hPARP-1 DBD	4.98 ± 0.03	0.41 ± 0.02	0.74 ± 0.03	2.75 ± 0.02	0.172 ± 0.003
	1.59 ± 0.07	0.40 ± 0.01	0.23 ± 0.02		
	0.34 ± 0.01	0.19 ± 0.01	0.02 ± 0.01		
hPARP-1 DBD and DNA	4.20 ± 0.03	0.19 ± 0.01	0.48 ± 0.04	1.66 ± 0.01	0.104 ± 0.003
	1.49 ± 0.04	0.54 ± 0.02	0.48 ± 0.02		
	0.22 ± 0.02	0.27 ± 0.01	0.04 ± 0.01		

[a] The fluorescence lifetimes (τ_i), the relative amplitudes (α_i), the fractional intensities (f_i), and the mean lifetimes ($\langle \tau \rangle$) are expressed as means ± the standard error of the mean for three experiments. The width of the distribution associated with each lifetime was found to be narrow under each condition, being less than 20% of the value of the lifetime. The mean lifetime was calculated with $\langle \tau \rangle = \sum \alpha_i \tau_i$. Excitation and emission wavelengths are 295 and 350 nm, respectively. hPARP-1 DBD and DNA concentrations are 1 and 1.5 μM, respectively. [b] Quantum yields of the free and bound protein upon excitation at 295 nm. The values are expressed as means ± the standard error of the mean for three experiments.
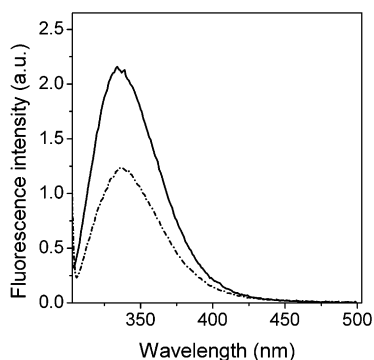

FIGURE 3: Fluorescence spectra of hPARP-1 DBD in the free state (—) and in the complex with a telomeric DNA end (-·-). The excitation wavelength was set at 295 nm.

Fluorescence spectra of hPARP-1 DBD are obtained by excitation at 295 nm where tryptophan is selectively excited. The fluorescence emission spectrum of the free protein displays a maximum at 332 nm. Since the four tryptophans are simultaneously excited, the emission spectrum of the protein constitutes an average of the fluorescence signal from four different emitters, and only global information can be obtained. The fluorescence maximum wavelength is significantly blue-shifted compared to that (350 nm) of fully exposed tryptophan (*23*), suggesting that the four Trp residues are mainly located in a nonpolar environment. Once the oligonucleotide binds, the fluorescence maximum wavelength remains unchanged (Figure 3). On the contrary, the fluorescence quantum yield of the Trp residues, which is 0.172 ± 0.003 in the free protein, decreases to 0.104 ± 0.003 in the complex, implying an ~40% quenching (Table 1).

To obtain further insight into the mechanism of protein−DNA interaction, we performed a time-resolved fluorescence study of hPARP-1 DBD in the absence and presence of an oligonucleotide. The fluorescence decay parameters of the free and DNA-bound protein are reported in Table 1. The fluorescence lifetimes of the protein show a trimodal distribution dominated by the longest lifetime of 4.98 ns which contributes ~75% to the total fluorescence. The mean lifetime of the free protein is 2.75 ns. Addition of the oligonucleotide leads to a decrease of 40% in the mean lifetime, in agreement with the extent of fluorescence quenching. This decrease is mainly due to a decrease in the amplitude of the long-lived lifetime, to the benefit of the amplitudes of the intermediate and short lifetimes. Moreover, the values of the long-lived and short-lived lifetimes are decreased to 4.20 and 0.22 ns, respectively.

Parameters for Binding of hPARP-1 DBD to a 5′ Recessed DNA Duplex. The interaction between hPARP-1 DBD and the double-stranded oligonucleotide mimicking a telomeric DNA end (Figure 2A) was investigated by monitoring the tryptophan fluorescence change upon addition of increasing oligonucleotide amounts. A systematic fluorescence decrease is observed until a plateau signal is reached at high DNA concentrations (inset of Figure 4A).

The titration experiment was repeated with four different initial protein concentrations (0.2, 0.45, 0.73, and 1 μM). In all cases, saturation is obtained with 0.5 equiv of oligonucleotide, indicating that two proteins are involved in the final complex. The stoichiometry of binding of hPARP-1 DBD to the telomeric DNA end is confirmed by a fluorescence anisotropy study (Figure 4B). Anisotropy is a suitable parameter for assessing the association of macromolecules since it varies in response to a change in the size and shape of the rotating molecules (*23*). Upon addition of increasing amounts of oligonucleotide, a remarkable increase in anisotropy is observed (Figure 4B). A stoichiometry of 2:1 is inferred for the protein−nucleic acid complex, in full agreement with the results of fluorimetric titration (inset of Figure 4B).

To exclude the possibility that the observed stoichiometry is due to a dimerization of hPARP-1 DBD prior to binding, we performed time-resolved fluorescence anisotropy experiments on the free hPARP-1 DBD. The longest rotational correlation time, θ_L, was found to be 13 ns (Figure 5). As previously discussed (*24*), tryptophanyl residues, despite their possible different local environments, can probe the rotation of the entire molecule. Therefore, the longest correlation time is associated with the overall tumbling of the molecule. A correlation time for the overall tumbling of 13 ns is very similar to 11.3 ns which is the expected rotational correlation time for a spherical molecule, whose molecular mass equals that of the monomeric hPARP-1 DBD (29 kDa) assuming 30% hydration (*23*). The correlation time of 13 ns corresponds to a hydration of 50%, a value which is not unlikely for a relatively small protein. Therefore, our results are not consistent with the existence of the hPARP-1 DBD dimer prior to DNA binding. In addition, electrospray mass spectroscopy experiments did not show any evidence of protein dimers. Taken together, these data indicate that hPARP-1 DBD is a monomer in the absence of DNA and dimerizes upon DNA binding. The behavior of hPARP-1 DBD appears to be similar to that of a designed protein consisting of the first and second zinc finger of Zif268
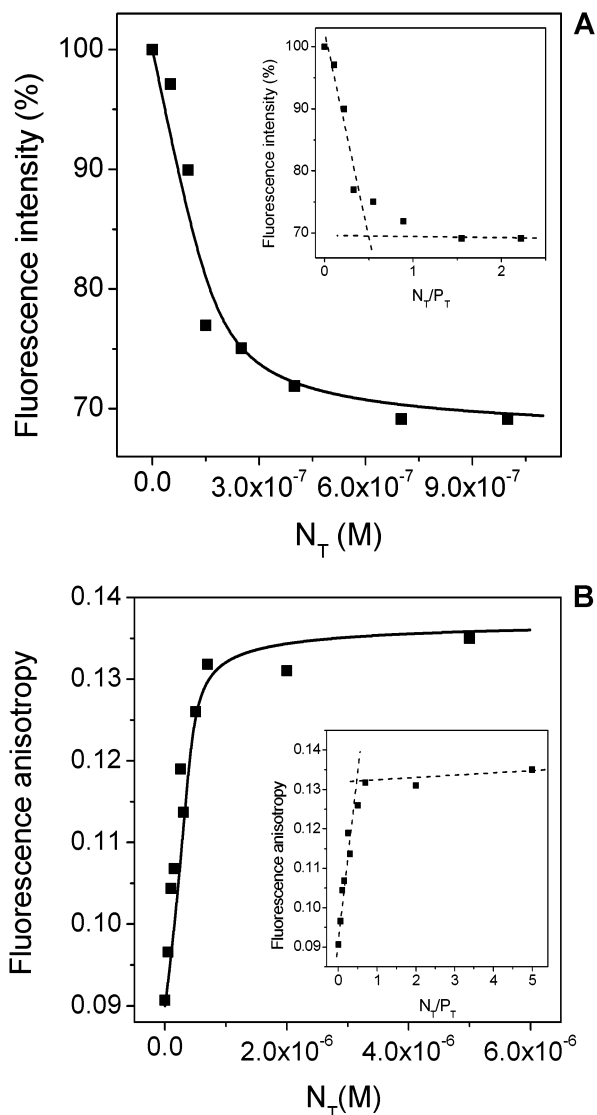
FIGURE 4: (A) Titration curve for binding of hPARP-1 DBD to the telomeric DNA end obtained with fluorescence intensity data. The solid line corresponds to the fit with the combination of eqs 4 and 5, as explained in the text. The inset shows the dependence of fluorescence intensity of hPARP-1 DBD on the DNA concentration. The concentration of hPARP-1 DBD was 0.45 μM. The linear parts of the binding curve are fitted and extrapolated separately with a linear curve fitting routine (- - -). The intersection indicates that the saturating DNA:protein ratio is 0.5. (B) Titration curve for binding of hPARP-1 DBD to the telomeric DNA end obtained with fluorescence anisotropy data. The solid line corresponds to the fit with the combination of eqs 5 and 6, as explained in the text. The inset shows the dependence of the fluorescence anisotropy of hPARP-1 DBD on the DNA concentration. The concentration of hPARP-1 DBD was 1 μM. The linear parts of the binding curve are fitted and extrapolated separately with a linear curve fitting routine (- - -). The intersection indicates that the saturating DNA: protein ratio is 0.5.

combined to the dimerization domain of GAL4 (*25*, *26*). It was shown that this protein is a monomer in solution and binds the predicted DNA site as a dimer, according to an "all-or-none" reaction (*27*). Our findings prompted us to assume that a similar all-or-none mechanism applies for the binding of hPARP-1 DBD to DNA with the following reaction scheme:
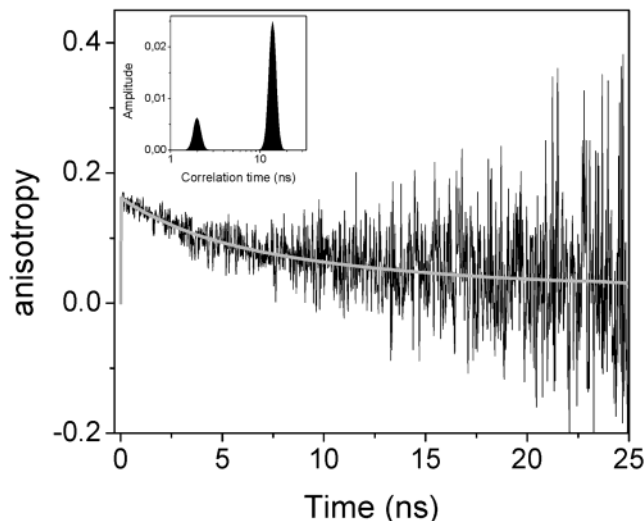
$$P + P + N \underset{}{\overset{K}{\rightleftharpoons}} PPN \qquad (3)$$

FIGURE 5: Fluorescence anisotropy decay of free hPARP-1 DBD at 20 °C. The peptide concentration was 0.73 μM in 50 mM Tris-HCl (pH 8), 100 mM NaCl, and 1 mM DTT. The measurement and the analysis were performed as described in Materials and Methods. The solid line represents the best fit using MEM. The experimental times were as follows: $\theta_1 = 1.2 \pm 0.8$ ns (associated amplitude of 0.14) and $\theta_2 = 13 \pm 1$ ns (associated amplitude of 0.86), corresponding to the local (θ_F) and the overall (θ_L) correlation times, respectively, according to eq 2. The inset shows the distribution of the correlation time as recovered by MEM analysis.

According to this scheme, the observed fluorescence can be expressed as follows:

$$F = F_P \frac{P}{P_T} + F_{PPN} \frac{KN_TP^2}{P_T(1 + KP^2)} \qquad (4)$$

where K represents the overall binding constant, F_P and F_{PPN} are the fluorescence signals of the free protein and the diprotein−nucleic acid complex, respectively, and P_T and N_T are the total protein and total nucleic acid concentrations, respectively. The total nucleic acid concentration varies at each point of the titration, while the total protein concentration is constant. The free protein concentration P is related to P_T, N_T, and K by the following cubic equation:

$$KP^3 + K(2N_T - P_T)P^2 + P - P_T = 0 \qquad (5)$$

The experimental fluorescence data are fitted to eq 4 by varying K. The free protein concentration is obtained from the roots of the third-order polynomial in eq 5 for each N_T when K was varied at a constant P_T. The roots were obtained using Laguerre's method (*28*). For each of the tested parameters, only one of the three roots was real and positive and could thus be identified with the free protein concentration. K was determined by minimizing χ^2 expressing the deviation between the experimental data and the evaluated curve. Applying global analysis to fluorescence data at four different protein concentrations, we obtained the best agreement between the experimental data and eq 4 for a K of 1.5×10^{14} M^{-2}.

To exploit anisotropy data, it is necessary to take into account the fact that the quantum yield changes as a function of the degree of binding. Accordingly, the observed fluorescence anisotropy is given by

$$r = \frac{r_{\mathrm{P}}P_{\mathrm{T}}(1 + KP^2) - 2KP^2N_{\mathrm{T}}(r_{\mathrm{P}} - r_{\mathrm{PPN}}s)}{P_{\mathrm{T}}(1 + KP^2) - 2KP^2N_{\mathrm{T}}(1 - s)} \quad (6)$$

where r_{P} and r_{PPN} represent the anisotropy of the free protein and the final complex, respectively, K represents the overall binding constant, and s is the ratio between the quantum yield of the bound and free protein (0.60 in this study). The free protein concentration in eq 6 is again linked to the binding parameters by eq 5. The procedure that was applied to fit the fluorescence data to eq 4 is now applied to fit the anisotropy data to eq 6. From a global analysis at two different total protein concentrations, we obtain a binding constant K of 7.3×10^{13} M^{-2} which is in good agreement with the value obtained from fluorescence intensity data. Finally, by applying a global analysis simultaneously to the fluorescence and the anisotropy data, we obtain a binding constant K of 1.4×10^{14} M^{-2}.

Panels A and B of Figure 4 show the fit of the fluorescence data to eq 4 and the fit of the anisotropy data to eq 6, respectively, using the binding constant determined from the simultaneous global analysis.

To determine the balance between ionic and nonionic interactions in complex formation, we performed a salt-back titration using fluorescence detection (Figure 6). The slope of log K versus log[NaCl] yields an m' of 2.7 ± 0.2, suggesting that approximately three ion pairs are formed in the complex. Moreover, $K(1 \text{ M}) = (4 \pm 1) \times 10^{11}$ M^{-2}, indicating that at 0.1 M NaCl the nonionic interactions represent ∼80% of the binding energy.

DISCUSSION

Fluorescence Properties of hPARP-1 DBD. We obtained structural and functional information about the zinc finger domain of hPARP-1 by studying its fluorescence properties. However, the number of fluorescent residues prevents a more detailed interpretation of the signal. The large blue shift detected in the wavelength of maximum emission of hPARP-1 DBD upon excitation at 295 nm indicates that Trp residues are mainly in a nonpolar environment. Indeed, the unusually long CCHC zinc fingers of hPARP-1 DBD as well as the very long spacer between them can favor folded structures in the free state, which can create hydrophobic pockets around tryptophans. Alternatively, a cluster of aromatic residues around the tryptophan can also lead to short wavelength fluorescence maxima (*29, 30*). Since in the hPARP-1 DBD sequence two of the Trp residues are flanked by a Tyr residue, this cluster effect may be relevant.

Binding of DNA to hPARP-1 DBD significantly reduces the fluorescence of the tryptophans in the protein. However, the interpretation of fluorescence data is limited in the case of multi-tryptophan proteins because the fluorescence signal cannot be resolved into the constituting individual emitters. Experiments with hPARP-1 DBD mutants in which one or more Trp residues are site-specifically mutated into non-fluorescent residues are in progress in an effort to overcome this limitation.

Binding of hPARP-1 DBD to a 5′ Recessed DNA Duplex. The DNA binding properties of hPARP-1 have been investigated using biochemical and spectroscopic approaches. DNA duplexes bearing a 5′ recessed end made of TTAGGG repeats mimicking a telomere end were used. Unexpectedly,
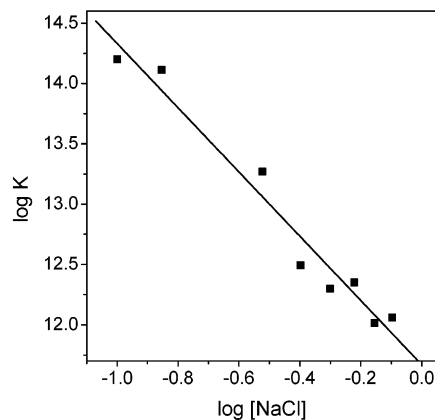

FIGURE 6: Log−log plot of the dependence of the overall binding constant K on NaCl concentration representing the back titration of the complex between hPARP-1 DBD to the 5′ recessed DNA end. Protein and oligonucleotide concentrations were 1 and 0.8 μM, respectively. The straight line represents the fit to the experimental data using eq 1, as explained in the text.

our results show that hPARP-1 or its zinc finger domain recognizes specifically a junction between double- and single-stranded DNA and not only a nick. An asymmetrical positioning of the protein, with respect to the 5′ end, was found, suggesting that hPARP-1 interacts mainly with the double-stranded portion of the DNA probe, whereas the single-stranded region appears to be less protected. This asymmetric type of binding is reminiscent of the binding mode of the bacterial histone-like protein HU that binds preferentially to junctions, nicks, and cruciforms, and like hPARP-1 bends its target DNA (*31*). It is likely that even in a single-stranded DNA nick, hPARP-1 recognizes mainly the 5′ end of the nick, leaving the 3′ end free of access to DNA 3′ end-processing enzymes that contribute to base excision repair. Similarly, it was found that PARP-2, alone and in partnership with TRF-2, binds the same type of telomeric structure (F. Dantzer *et al.*, manuscript submitted for publication).

The possible location of hPARP-1 at a telomeric end *in vivo* fully supports the protecting function of this enzyme that also extends to other homologues such as Tankyrase-1 involved in telomere maintenance (*32*). The PARP-like zinc finger family now comprises three DNA repair enzymes bearing one (DNA ligase III), two (hPARP-1), or three (3′-phosphoesterase) conserved zinc fingers. Interestingly, these enzymes seem to have evolved a functional module specialized in the recognition of 5′ or 3′ DNA ends. Clearly, the three-dimensional structure of this module will be of interest.

The binding of hPARP-1 DBD to the telomeric DNA end (Figure 2A) has been followed by monitoring the fluorescence emission upon selective excitation of the Trp residues. Consequently, the quenching of hPARP-1 DBD fluorescence after the addition of DNA is related exclusively to the emission of the Trp residues of the protein, implying the involvement of at least one tryptophan in the DNA binding process.

Interestingly, all the binding experiments show unambiguously that the stoichiometry of the DNA−hPARP-1 DBD complex is two proteins per one nucleic acid. On the other hand, the presence of a free dimeric form of this protein is excluded by time-resolved anisotropy, implying that hPARP-1 DBD does not bind as a preformed dimer. Even if intermo-

lecular tryptophan−tryptophan energy transfer can cause depolarization, it should not affect the longest correlation time of free hPARP-1 DBD. In fact, the energy transfer is a fast process that cannot compete with such a long correlation time. Therefore, from the longest correlation time of 13 ns (Figure 5) which is close to the expected value for a spherical molecule of 29 kDa, we conclude that hPARP-1 DBD is a monomer in the concentration range of 0.2−1 μM. This is the concentration range used in this study and corresponds to the physiological concentration of hPARP-1 in the nucleus (*33*). Moreover, a previous study (*34*) reports that free hPARP-1 dimerizes up to 40% only at a concentration of ∼12 μM, and extrapolating from these data, only 5% of the proteins form dimers at 1 μM, in line with our conclusion.

The constant for binding of hPARP-1 DBD to an oligo-nucleotide mimicking a telomeric DNA end (1.4×10^{14} M^{-2}) is second-order. This feature is typical for proteins that exist as a monomer and bind the DNA site as a dimer, as depicted in eq 3 (*25, 26*).

The DNA complex of hPARP-1 DBD is strongly stabilized by nonionic interactions, a hallmark of binding specificity (*35*). These interactions may notably involve Trp residues. Information about the role of the Trp residues in the binding process is obtained by the time-resolved fluorescent investigation. In the presence of a saturating DNA concentration, the major feature is the decrease in the amplitude of the longest lifetime to the benefit of the others. The average radiative rate constant which corresponds to the ratio of the quantum yield and the average lifetime does not change after DNA binding (Table 1). This result excludes a pure static quenching mechanism consisting of the formation of a nonfluorescent complex between the fluorophore and the quencher for all the Trp residues (*23*). Consequently, the observed amplitude redistribution can be attributed essentially to population reshuffling (*29*). Noticeably, the microconformations where tryptophans are more quenched are preferentially selected upon binding to DNA. Despite the number of Trp residues which prevents a clear interpretation, these results are in line with the involvement of one tryptophan in the stacking interaction with the DNA bases, a situation where the Trp residue is strongly quenched (*36*). The stacking interaction involves mainly London dispersion forces and a hydrophobic contribution. Therefore, it is essentially nonionic in nature (*37, 38*). Accordingly, the evidence that nonionic interactions constitute the major contribution to the binding energy corroborates the hypothesis that Trp stacking plays an important role in the stability of the DNA complex of hPARP-1 DBD. A critical role of Trp stacking during nucleic acid binding was already asserted for the tryptophan located in the distal zinc finger of HIV-1 NCp7 (*39, 40*). Moreover, Trp residues stack preferentially with the bases of single-stranded nucleic acids (*35*), which suggests that stacking may be a driving event in the DNA nick recognition promoting the interaction with the single-strand portion. Nevertheless, a part of the fluorescence decrease for hPARP-1 DBD is also associated with a limited decrease in the lifetimes upon binding. This observation suggests that some Trp residues are affected by conformational changes (without stacking), where dynamic quenching is favored. Dynamic quenching is a time-dependent process resulting from diffusive encounters between the fluorophore and quenchers during the lifetime of the excited state (*23*). This complex behavior can

be the sign that more than one tryptophan residue is involved in the binding process. Each peak in the trimodal lifetime distribution can indeed result from the collapse of lifetimes of different Trp residues. Such a collapse originates from the limitations of the time-resolved measurements and data analysis, which preclude resolution of components that differ by less than a factor of ∼1.5 (*41*). In this context, we can imagine that the recorded time-resolved profile contains the signal of at least two major classes of contributing Trp residues: one class is involved in a stacking interaction and the other is affected principally by conformational modification of its environment due to the binding process.

Our study opens new perspectives for interpreting the selective binding of hPARP-1 to its nucleic acid target. We found that the zinc finger domain of hPARP-1 is able to recognize specifically the junction between the double and single strand in a DNA duplex bearing a 5′ recessed end. Stacking of Trp residues with the DNA seems to play an important role in the recognition of the DNA structure. Interestingly, protein dimerization occurs at the same time as binding. As shown by the footprint experiment, hPARP-1 is asymmetrically positioned at the 5′ end (Figure 2A), in line with the formation of a hPARP-1 catalytic dimer which can be asymmetric also in terms of activity (*42*): one molecule behaving as a donor of poly(ADP-ribose) and the other being an acceptor. The cooperativity originating from dimerization narrows the concentration range over which binding occurs, resulting in a sharp transition between "on" and "off" regulatory states.

REFERENCES

1. Zhou, B. B., and Elledge, S. J. (2000) *Nature 408*, 433−439.
2. de Murcia, G., and Shall, S. (2000) *From DNA damage and stress signalling to cell death. Poly ADP-ribosylation reactions*, Oxford University Press, New York.
3. D'Amours, D., Desnoyers, S., D'Silva, I., and Poirier, G. G. (1999) *Biochem. J. 342* (Part 2), 249−268.
4. Simbulan-Rosenthal, C. M., Haddad, B. R., Rosenthal, D. S., Weaver, Z., Coleman, A., Luo, R., Young, H. M., Wang, Z. Q., Ried, T., and Smulson, M. E. (1999) *Proc. Natl. Acad. Sci. U.S.A. 96*, 13191−13196.
5. Dantzer, F., Schreiber, V., Niedergang, C., Trucco, C., Flatter, E., De La Rubia, G., Oliver, J., Rolli, V., Menissier-de Murcia, J., and de Murcia, G. (1999) *Biochimie 81*, 69−75.
6. de Murcia, J. M., Niedergang, C., Trucco, C., Ricoul, M., Dutrillaux, B., Mark, M., Oliver, F. J., Masson, M., Dierich, A., LeMeur, M., Walztinger, C., Chambon, P., and de Murcia, G. (1997) *Proc. Natl. Acad. Sci. U.S.A. 94*, 7303−7307.
7. Beneke, R., Geisen, C., Zevnik, B., Bauch, T., Muller, W. U., Kupper, J. H., and Moroy, T. (2000) *Mol. Cell. Biol. 20*, 6695−6703.
8. Doucet-Chabeaud, G., Godon, C., Brutesco, C., de Murcia, G., and Kazmaier, M. (2001) *Mol. Genet. Genomics 265*, 954−963.
9. Taylor, R. M., Whitehouse, C. J., and Caldecott, K. W. (2000) *Nucleic Acids Res. 28*, 3558−3563.
10. Petrucco, S., Volpi, G., Bolchi, A., Rivetti, C., and Ottonello, S. (2002) *J. Biol. Chem. 277*, 23675−23683.
11. Eftink, M. R. (1997) *Methods Enzymol. 278*, 221−257.
12. Cao, Y., Li, H., Deb, S., and Liu, J. P. (2002) *Oncogene 21*, 3130−3138.

13. Deng, Z., Lezina, L., Chen, C. J., Shtivelband, S., So, W., and Lieberman, P. M. (2002) *Mol. Cell 9*, 493−503.

14. Gradwohl, G., Menissier de Murcia, J., Molinete, M., Simonin, F., and de Murcia, G. (1989) *Nucleic Acids Res. 17*, 7112.

15. Molinete, M., Vermeulen, W., Burkle, A., Menissier-de Murcia, J., Kupper, J. H., Hoeijmakers, J. H., and de Murcia, G. (1993) *EMBO J. 12*, 2109−2117.

16. Menissier-de Murcia, J., Molinete, M., Gradwohl, G., Simonin, F., and de Murcia, G. (1989) *J. Mol. Biol. 210*, 229−233.

17. Eisinger, J., and Navon, G. (1969) *J. Chem. Phys. 50*, 2069−2077.

18. Record, M. T., Jr., Lohman, M. L., and De Haseth, P. (1976) *J. Mol. Biol. 107*, 145−158.

19. Livesey, A. K., and Brochon, J. C. (1987) *Biophys. J. 52*, 693−706.

20. Gradwohl, G., Menissier de Murcia, J. M., Molinete, M., Simonin, F., Koken, M., Hoeijmakers, J. H., and de Murcia, G. (1990) *Proc. Natl. Acad. Sci. U.S.A. 87*, 2990−2994.

21. de Lange, T. (2002) *Oncogene 21*, 532−540.

22. Vuilleumier, C., Maechling-Strasser, C., Gerard, D., and Mely, Y. (1997) *Anal. Biochem. 244*, 183−185.

23. Lakowicz, J. R. (1983) *Principles of fluorescence spectroscopy*, Wiley, New York.

24. Bialik, C. N., Wolf, B., Rachofsky, E. L., Ross, J. B., and Laws, W. R. (1998) *Biophys. J. 75*, 2564−2573.

25. Pomerantz, J. L., Wolfe, S. A., and Pabo, C. O. (1998) *Biochemistry 37*, 965−970.

26. Wang, B. S., and Pabo, C. O. (1999) *Proc. Natl. Acad. Sci. U.S.A. 96*, 9568−9573.

27. Cantor, R. C., and Schimmel, P. R. (1980) *Biophysical Chemistry Part III*, Freeman Press, San Francisco.

28. Press, W. H., Teukolsky, S. A., Vetterling, W. T., and Flannery, B. P. (1992) *Numerical Recipes in C*, 2nd ed., Cambridge University Press, Cambridge, U.K.

29. Engelborghs, Y. (2001) *Spectrochim. Acta, Part A 57*, 2255−2270.

30. Gopalan, V., Golbik, R., Schreiber, G., Fersht, A. R., and Altman, S. (1997) *J. Mol. Biol. 267*, 765−769.

31. Kamashev, D., and Rouviere-Yaniv, J. (2000) *EMBO J. 19*, 6527−6535.

32. Cook, B. D., Dynek, J. N., Chang, W., Shostak, G., and Smith, S. (2002) *Mol. Cell. Biol. 22*, 332−342.

33. Mellors, R. C., Kupfer, A., and Hollender, A. B. (1953) *Cancer 6*, 372−384.

34. Bauer, P. I., Buki, K. G., Hakam, A., and Kun, E. (1990) *Biochem. J. 270*, 17−26.

35. Helene, C., and Maurizot, J. C. (1981) *CRC Crit. Rev. Biochem. 10*, 213−258.

36. Montenay-Garestier, T., Toulme, F., Fidy, J., Toulme, J. J., Le Doan, T., and Helene, C. (1983) Structure and dynamics of peptide-nucleic acid complexes, in *Structure, dynamics, interactions and evolution of biological macromolecules* (Hélène, C., Ed.) pp 113−128, D. Reidel Publishing Co., Dordrecht, The Netherlands.

37. Kumar, N. V., and Govil, G. (1984) *Biopolymers 23*, 2009−2024.

38. Bloomfield, V. A., Crothers, D. M., and Tinocco, I. (1999) *Nucleic acids: structures, properties, and functions*, University Books, Sausalito, CA.

39. Vuilleumier, C., Bombarda, E., Morellet, N., Gerard, D., Roques, B. P., and Mely, Y. (1999) *Biochemistry 38*, 16816−16825.

40. Bombarda, E., Ababou, A., Vuilleumier, C., Gerard, D., Roques, B. P., Piemont, E., and Mely, Y. (1999) *Biophys. J. 76*, 1561−1570.

41. Vix, A., and Lami, H. (1995) *Biophys. J. 68*, 1145−1151.

42. Mendoza-Alvarez, H., and Alvarez-Gonzalez, R. (1993) *J. Biol. Chem. 268*, 22575−22580.